nature communications

Article

https://doi.org/10.1038/s41467-026-70123-w

Lasing-like dynamics with virtual gain driven by complex-frequency excitations

Received: 6 August 2025

Accepted: 18 February 2026

Published online: 03 March 2026

Check for updates

Boyi Xue[1], Ruixiang Zhang[1], Yicheng Zhu[1], Yuncong Sun[1], Xianfeng Chen[2], Andrea Alù[3,4] & Wenjie Wan[1,2]

Complex-frequency excitation controls non-Hermitian light-matter interactions by temporally shaping signals to bypass inherent material gain or loss constraints. While virtual loss has enabled coherent perfect absorption, its time-reversed counterpart: virtual gain, remains less explored in optical systems. Here, we theoretically and experimentally demonstrate lasing-like dynamics in a passive whispering-gallery-mode microcavity using complex-frequency excitations. Virtual gain counteracts intrinsic material and radiation losses, producing an instantaneous transmittance that exceeds unity and saturates at a quasi-steady value. Beyond a critical threshold-like point, the system enters a regime of divergent, exponentially growing response, mimicking the transient buildup of a real laser without requiring population inversion or active media. This linear effect allows for the robust coexistence of lasing-like behavior and perfect absorption, with transitions controlled by virtual gain tuning. These results establish a versatile framework for manipulating non-Hermitian interactions in passive platforms, offering remarkable potential for applications in sensing, optical communications, and energy storage.

Lasers use light amplification by stimulated emission of radiation to emit intense and coherent beams of light. This property makes them indispensable in various applications. Conventionally, the amplification of a laser is enabled by a gain medium, in which excited atoms or molecules by external pumping, provide sufficient gain to overcome losses to achieve lasing[1–4]. The required level of gain is material-dependent and limited by the physical gain medium. Alternatively, complex-frequency excitations (CFEs)[5–9] enable virtual gain or loss in a linear system by tailoring the incoming excitation signal in time, circumventing the limitations of material gain or loss. This approach offers an interesting playground for various applications in optics[5,6], acoustics[10,11], electronics[12–14], microwave radiation[15–17], metasurfaces[18], and integrated photonics[19,20]. Broadly, CFEs enable tailorable non-Hermitian responses, which can support coherent virtual absorption (CVA), virtual critical coupling[5,6,11,15–23], virtual parity-time symmetry[12,13,24,25], optical pulling forces[26], and exotic light scattering[27]. Recent works have demonstrated that such CFEs can compensate for material losses in superlenses[28–31], offering an interesting framework for multidisciplinary engineering solutions to overcome material constraints.

While coherent perfect absorption enabled by CFEs has been demonstrated through virtual loss, its time-reversed counterpart[4,32,33], a lasing-like scattering regime enabled by virtual gain, has remained for the most part unexplored[27]. These two dual scenarios correspond respectively to the excitation of complex zeros and poles of the S-matrix of a linear system[7]. Under an $e^{-i\omega t}$ convention, the poles of a passive system are always located in the lower half of the complex frequency plane, corresponding to exponentially divergent response in time, while zeros lie in the upper half-plane in the Hermitian limit, corresponding to exponential attenuation. By adding a specific amount of material loss, it is possible to push one of these zeros to the real axis, enabling coherent perfect absorption[34]. Virtual loss, enabled

[1]State Key Laboratory of Photonics and Communications Global College, Shanghai Jiao Tong University, Shanghai, China. [2]Department of Physics and Astronomy, Shanghai Jiao Tong University, Shanghai, China. [3]Photonics Initiative, Advanced Science Research Center, City University of New York, New York, NY, USA. [4]Physics Program, Graduate Center, City University of New York, New York, NY, USA. e-mail: aalu@gc.cuny.edu; wenjie.wan@sjtu.edu.cn

by tailored CFEs, can replace the material loss and support similar CVA through CFEs[5,6,11,15–23]. The dual of this phenomenon, based on virtual gain, has been proposed to counteract losses in plasmonic and phononic materials, enabling super-resolution imaging[28–31], long-range propagation[35], slow light[36–39], ultrasensitive molecular sensing[40], superscattering[27], and virtual parity-time symmetry[12,13,24,25]. The concept has also been extended to acoustic systems to access and tailor non-Hermitian sound interactions with materials[10,11]. However, the experimental demonstration of lasing-like dynamics utilizing virtual gain has remained elusive.

In this work, we demonstrate lasing-like dynamics through CFEs in an ultra-high quality (Q) factor whispering-gallery-mode optical microcavity. In line with previous virtual critical coupling implementations[6,19,20], our approach employs an exponentially decaying excitation signal that induces virtual gain, thereby enabling dynamic modulation of the transmission features at the transmission/drop port. We investigate lasing-like responses and identify a threshold-like transition point—defined as the condition where the engineered virtual gain exactly balances the total system loss and accesses the complex pole of the system. Before reaching this threshold, the instantaneous amplitude transmittance after a transient saturates at a quasi-steady level that can far exceed unity, indicating that the scattered optical field can be stably amplified in a manner analogous to an active device. As the virtual gain approaches the threshold level, the system never reaches a quasi-steady state, and exactly at the threshold, as in a laser, the transmission grows linearly. Past threshold, the system response diverges, similar to a laser past threshold before nonlinearities kick in, with a pronounced amplification reminiscent of the transient buildup phase in a real laser. Since our system is based on a fully linear response, our lasing-like dynamics remain fundamentally distinct from conventional lasing in that they do not experience gain saturation or other nonlinear dynamics. Thus, the divergent regime past the threshold still obeys energy conservation and can be accessed within a stable response. The same platform also enables coherent virtual absorption (CVA) in the under-coupled cavity regime. As the virtual gain increases, the system undergoes successive coupling-state transitions: initially under-coupled, then critically coupled (CVA), and then over-coupled, ultimately entering a lasing-like state when the gain exceeds the threshold point. Our work provides key advances in the context of complex frequency applications, with implications both for fundamental physics and for practical applications. These findings demonstrate an exciting pathway to access lasing-like regimes in a tunable fashion without relying on active media, enhancing and controlling light-matter interactions beyond the limits imposed by material passivity, and paving the way for various applications such as noninvasive sensing, energy storage, and nanoscale light manipulation.

Results

Theoretical analysis of lasing-like dynamics

The schematic illustration of our lasing-like system is depicted in Fig. 1. A centimeter-sized microcavity with an ultra-high quality factor is coupled to two optical fibers on both sides, forming an add-drop configuration. The system is excited with temporally shaped exponentially decaying pulses, and the output signal at the drop port is measured and analyzed, as shown in Fig. 1a. κ_i is the intrinsic loss rate of the microcavity, while κ_1, κ_2 denote the coupling rate to the input and drop port fibers, respectively. The amplitude of the incoming pulse is a_{in} and the outcoupled signal at the drop port is a_{out}. The time evolution of the signal can be effectively described using temporal coupled mode theory (TCMT). The equation of motion for the intracavity field a can be written as[32,33,41]

$$\frac{da(t)}{dt} = -(\kappa + i\omega_0)a(t) + \sqrt{2\kappa_1}a_0 e^{-i\omega_L t} \tag{1}$$

where $\kappa = \kappa_i + \kappa_1 + \kappa_2$ is the total loss rate, ω_0 is the resonant frequency, ω_L is the laser frequency.

We assume that the excitation signal oscillates at a complex frequency $a_{in}(t) = a_0 e^{-i\omega_L t}$, where $\omega_L = \omega_{re} + i\omega_{im}$. The imaginary part ω_{im} indicates the growth or decay rates of the signal amplitude modulation. In our experiment, we consider $\omega_{im} < 0$ and $g = -\omega_{im}$ represents the virtual gain. The amplitude of the output signal at the drop port is $a_{out}(t) = \sqrt{2\kappa_2}a(t)$. We can solve Eq. (1) and get an analytical solution for a_{out}. The ratio between the amplitude of output and input signals, which is referred to as the amplitude transmittance, can be written as

$$T(t) = \left|\frac{a_{out}(t)}{a_{in}(t)}\right| = \left|\frac{2\sqrt{\kappa_1\kappa_2}}{\kappa + \omega_{im} + i\Delta}(1 - e^{-(\kappa + \omega_{im} + i\Delta)t})\right| \tag{2}$$

Here $\Delta = \omega_0 - \omega_{re}$ is the frequency detuning of the mode. The transmittance exhibits generally time-dependent dynamics, governed by the eigenfrequency position in the complex plane. For real-frequency excitations in passive systems, the amplitude transmittance $T(t)$ converges to a quasi-steady state as $t \to \infty$, since the transient phenomena all decay in time. By considering CFEs with exponentially decaying input pulses, we can introduce virtual gain in the system. This enables accessing complex poles in the lower complex half plane. We can therefore expect to access quasi-steady state regimes described by Eq. (2) with values far exceeding unity, and even

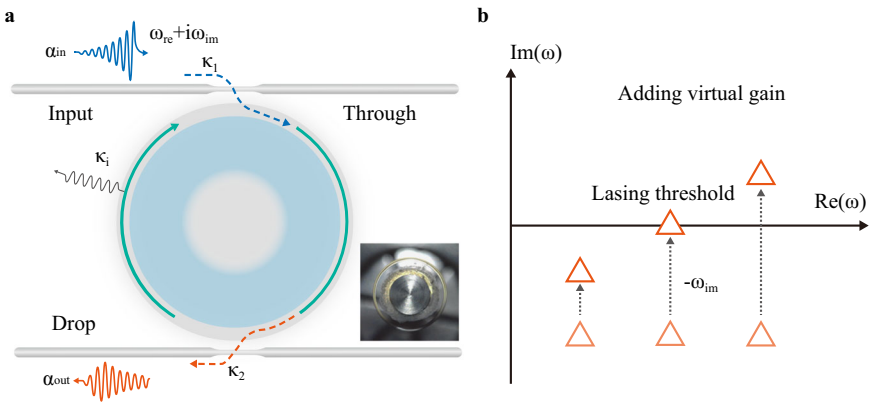

Fig. 1 | Conceptual illustration of a system exhibiting lasing-like dynamics. **a** Schematic diagram of a microcavity with intrinsic loss κ_i coupled to two fibers with coupling rates κ_1 and κ_2, respectively. An exponentially decaying pulse with a decay rate ω_{im} is launched through the input port to excite the resonator. The output signal is measured at the drop port. **b** Complex-frequency analysis of the drop-port transmittance, showing the scattering pole initially located in the lower half-plane. Introducing virtual gain through complex-frequency excitations shifts the poles towards the real axis, enabling lasing-like dynamics.

https://doi.org/10.1038/s41467-026-70123-w

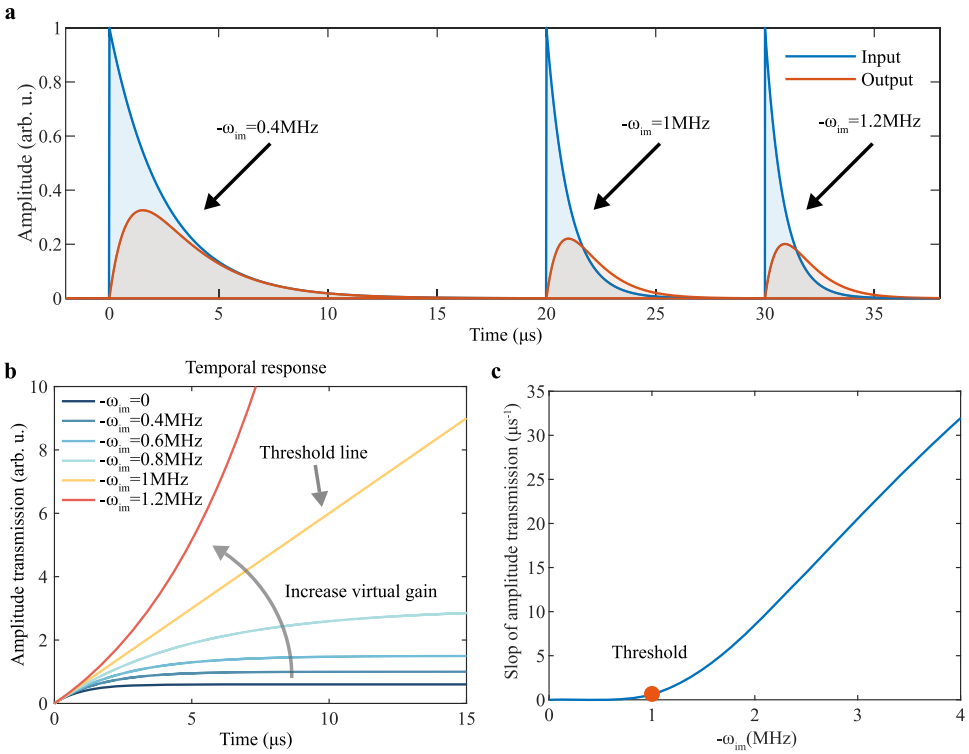

Fig. 2 | Theoretical analysis of lasing-like dynamics in a microcavity. **a** Illustration of input (blue) and output (red) pulses at $\Delta = 0$ under various excitation scenarios. The total loss rate of the system is set to be $\kappa = 1MHz$. The below-threshold scenario is demonstrated at $-\omega_{im} = 0.4MHz$, the threshold-like transition is demonstrated at $-\omega_{im} = 1MHz$, and the above-threshold scenario is demonstrated at $-\omega_{im} = 1.2MHz$. **b** Simulated amplitude transmission $T(t)$ plotted as a function of time for different levels of virtual gain. For moderate values of virtual gain, the transmission coefficient reaches a quasi-steady state, with larger levels for larger gain. When the virtual gain reaches the threshold-like transition, $T(t)$ exhibits linear growth, and for larger gain values, it exponentially grows, indicating the breakdown of the quasi-steady state and the onset of lasing-like effects. **c** Slope of amplitude transmission $T(t)$ at $\Delta = 0$ and $t = -5.3/\omega_{im}$ plotted as a function of virtual gain. A transition point can be observed, analogous to a conventional laser.

regimes for indefinite growth of the instantaneous transmission over time, despite the absence of physical gain media.

In a conventional laser, lasing can be accessed by engaging a pole of the scattering matrix in the complex-frequency plane. As the gain approaches its threshold value, this pole moves toward the real frequency axis, implying the onset of self-sustained oscillations. Similarly, the use of complex frequency excitations with a decaying exponential amplitude allows us to access the natural resonances of our passive system, whose self-oscillations decay in time due to the natural material and radiation loss. By exciting the system with a similar complex frequency, we can observe phenomena analogous to self-oscillations, driven by the stored energy introduced in the system during the transient, and we observe clear lasing-like temporal dynamics. As illustrated in Fig. 1b, the divergent response of the instantaneous transmission in our system corresponds to accessing a pole in the complex-frequency plane, analogous to a laser. While material gain shifts the poles of a passive system towards the real axis, a similar effect can be achieved using complex-frequency excitations if the virtual gain compensates the cavity loss, leading to a transition from convergent to divergent response in the transmittance $T(t)$. This is a lasing-like effect which mimics material gain, and the transition point between quasi-steady state response and divergent response follows the same linear dynamics of a laser at threshold, with a linearly growing evolution of the instantaneous transmission.

By setting $\Delta = 0$ in Eq. (2), which corresponds to resonant excitation at the zero-detuning condition, we simulate the temporal dynamics of the input pulse and drop-port output as we vary the virtual gain. We can define three scenarios (Supplementary Note 1): below the threshold point (virtual gain is less than total loss), at the threshold (virtual gain equals total loss), and above the threshold point (virtual gain exceeds total loss). Under the condition that $t \gg 0$, the transmission coefficient exhibits distinct behaviors for these three scenarios, and Eq. (2) can be explicitly rewritten as

$$T(t) \to \begin{cases} \frac{2\sqrt{\kappa_1\kappa_2}}{\kappa + \omega_{im}} & -\omega_{im} < \kappa \ (below\ threshold\ point) \\ 2\sqrt{\kappa_1\kappa_2}t & -\omega_{im} = \kappa \ (at\ threshold\ point) \\ -\frac{2\sqrt{\kappa_1\kappa_2}}{\kappa + \omega_{im}} e^{-(\kappa + \omega_{im})t} & -\omega_{im} > \kappa \ (above\ threshold\ point) \end{cases} . \quad (3)$$

As evident from Eq. (3), the tailored pulse is amplified instantaneously in the presence of virtual gain, while $T(t)$ shows different dynamics in the three scenarios. The simulation results for the geometry of Fig. 1 are presented in Fig. 2a, showing the time-domain waveforms of input and output pulses at zero detuning for these three gain regimes. Their instantaneous ratio—the time evolution of the zero-detuning amplitude transmission coefficient $T(t)$—is plotted in Fig. 2b, and it is consistent with Eq. (3). The total loss rate is set to 1MHz, with parameters $\kappa_i = 0.4\text{MHz}, \kappa_1 = 0.3\text{MHz}, \kappa_2 = 0.3\text{MHz}$. As illustrated above, the threshold point is at $-\omega_{im} = \kappa = 1\text{MHz}$. These scenarios are illustrated at $-\omega_{im} = 0.4\text{MHz}$, $-\omega_{im} = 1\text{MHz}$ and $-\omega_{im} = 1.2\text{MHz}$, respectively. When virtual gain remains below the threshold, $T(t)$ grows rapidly in time and eventually stabilizes at a steady value. This steady value increases as the virtual gain grows, and it can far exceed unity, indicating that the scattered optical field becomes substantially stronger than the incident field at the same instant in the quasi-steady state. The underlying mechanism for this gain-like response involves the resonant mode of the cavity, which temporarily stores energy during the transient phase and subsequently releases it in the quasi-steady state. Through appropriate tailoring of the input waveform, this release can enhance the resonant

response. This behavior closely mirrors the transient amplification followed by gain saturation observed in conventional lasers below threshold as they reach steady-state emission, yet it occurs in a fully passive system driven by virtual gain. When the threshold point is reached, the decay rate of the excitation meets and then exceeds the energy release rate of the resonant mode. As the excitation weakens, the cavity continues to release the stored energy at a slower rate, preventing the system from reaching equilibrium. Consequently, the transmittance grows linearly in time at threshold, and then exponentially. Indeed, with further increase in virtual gain, balancing becomes even less attainable, and the transmittance grows exponentially, reflecting extremely strong dynamic amplification of the input pulse. This divergent amplification originates from a mismatch between the input decay rate and the cavity decay rate, resembling the transient buildup in a real laser but lacking nonlinear saturation. In conventional lasers, such a condition would lead to instabilities that are compensated by nonlinearities. In our system, however, the absence of actual gain and the exponentially decaying excitation ensure that unlimited amplification does not cause instabilities or nonlinearities.

The apparent growth of $T(t)$ may appear to violate energy conservation. It is important to clarify that $T(t)$ is a normalized instantaneous ratio, not a direct measure of total energy radiated by the resonator over time. Its increase reflects a temporal reshaping of power, where the output decays more slowly than the input, rather than energy creation. Because $|a_{in}(t)|$ itself is decaying exponentially in time, the absolute instantaneous output power $|a_{out}(t)|^2$ remains small and continues to decay over time even when $T(t) \gg 1$. In fact, the total pulse energies E_{in} and E_{out}, defined as the time integrals of instantaneous power across the entire duration of the excitation, indeed obey energy conservation. Since $\omega_{im} < 0$ and $\kappa = \kappa_i + \kappa_1 + \kappa_2$, we obtain

$$\frac{E_{out}}{E_{in}} = \frac{\int_0^\infty |a_{out}(t)|^2 dt}{\int_0^\infty |a_{in}(t)|^2 dt} = \frac{4\kappa_1\kappa_2}{\kappa(\kappa - \omega_{im})} \le \frac{4\kappa_1\kappa_2}{\kappa^2} \le \frac{4\kappa_1\kappa_2}{(\kappa_1+\kappa_2)^2} \le 1 \quad (4)$$

Thus, the output energy remains finite and never exceeds the input energy, confirming that the system is passive, linear, and fully consistent with energy conservation (Supplementary Note 6).

Besides the absolute value of the transmission coefficient, we were also interested in studying its time evolution, which can be illustrated by the slope of the curves in Fig. 2b. The time derivative of the transmission $T(t)$ reveals the system's effective amplification and degree of divergence. A natural approach is to study the time derivative of the transmission at a fixed time as a function of virtual gain (Supplementary Note 3). However, an ideal exponential decay signal cannot be generated experimentally, due to practical limitations. Our actual input signal is a pulse with finite duration, which decays to a specific value before transitioning into the next pulse period (decaying to approximately 0.5% of its peak amplitude in our experiment). Measuring the slope of $T(t)$ at a fixed time is impractical because this time may exceed the pulse period. Consequently, we analyzed the transmittance at $t = -5.3/\omega_{im}$, the time when the input amplitude decays to 0.5% of its peak value. In Fig. 2c, we plot the slope of $T(t)$ at $\Delta = 0$ as a function of virtual gain. It is evident that the time derivative is zero for small virtual gains, corresponding to the quasi-steady state. When the virtual gain exceeds the threshold $-\omega_{im} = \kappa$, the time derivative increases rapidly, indicating a substantial enhancement in the amplification factor and a more pronounced divergence trend as the virtual gain increases. This behavior resembles that of a traditional laser, where stimulated radiation begins at the lasing threshold, changing the temporal dynamics of the system response.

Experimental demonstration

In our experiment, a CaF_2 microcavity with a diameter of 1 millimeter and an ultra-high Q-factor of $10^8 \sim 10^9$ was fabricated through precise polishing. This microcavity was then coupled to two tapered fibers, which were fabricated from standard single-mode fibers in the telecom band, forming an add-drop microcavity system. The entire device was placed inside a vacuum-sealed metal box to ensure environmental stability. We performed both ring-down measurements and frequency-domain linewidth characterizations to determine the Q factor. The agreement between the two independent methods ensures measurement accuracy and guards against potential disturbances such as thermal effects that could otherwise distort the modal linewidth. We first characterized the cavity using cavity ring-down measurements. A square wave pulse with a sharp falling edge was launched into the cavity, allowing us to extract the cavity lifetime from the decaying optical fields using an oscilloscope, as shown in Fig. 3a. Additionally, we launched a monochromatic continuous wave into the cavity to record its transmission spectrum under real-frequency excitations. The power transmission spectrum at the drop port is shown in Fig. 3b, while the spectrum at the through port is shown in the inset of Fig. 3b. These measurements fully characterize the optical response of the add-drop system, providing both the intrinsic loss rate and coupling rate. The measured cavity lifetime $\tau = 1/\kappa = 0.522\mu s$ allows us to estimate the total loss to be $\kappa = 1.92$MHz. Since the selected mode resonates near a wavelength of 1560 nm, we estimate the loaded quality (Q) factor to be approximately $Q = \omega/(2\kappa) = 3.17 \times 10^8$, which can also be derived from the measured full wave half maximum ($\Delta\omega = 2\pi \times 0.61$MHz) in Fig. 3b. Given the measured transmittances of 0.27 and 0.23 at the drop and through ports, respectively, we can estimate the intrinsic loss and external coupling rates to be $\kappa_i = 0.92$MHz, $\kappa_1 = 0.5$MHz, $\kappa_2 = 0.5$MHz.

For the pulse measurements, the experimental setup is shown in Supplementary Fig. 1. A continuous laser centered at approximately 1560 nm was modulated via an electro-optic modulator (EOM), enabling precise shaping of the input intensity. The generated exponentially decaying pulse sequence was launched into the input port, while the output signal at the drop port was detected by a photodetector and recorded on an oscilloscope. Owing to the ultra-high Q factor and ultra-long lifetime of our microcavity, neither a high-speed modulator nor a fast oscilloscope was required. A 50:50 coupler was employed to split the incoming pulse into two paths: one exciting the cavity, while the other served as the reference for the input signal and was measured on the oscilloscope. Our focus lies on the response at the zero detuning point. However, locking the laser to the cavity resonance is challenging due to the narrow resonant linewidth resulting from the high Q factor and the weak thermal effect (hard-to-use thermal locking) caused by the large size of the microcavity. Consequently, we modulated the laser frequency using a 20 Hz triangular wave to scan around the resonant mode, concentrating solely on the pulse located at the zero detuning point. We recorded the input and output pulse intensities for three selected example complex excitation frequencies, as depicted in Fig. 3d–f. The region below the transition point is demonstrated at $-\omega_{im} = 1.14$MHz, the near-threshold scenario is illustrated at $-\omega_{im} = 1.99$MHz, and the above-threshold scenario is shown at $-\omega_{im} = 2.47$MHz. Their corresponding relative amplitude transmission $T(t)$ is plotted as a function of time in Fig. 3g–i. The time evolution of transmittance exhibits quasi-steady-state saturated amplification, linear growth, and exponential growth in the aforementioned three scenarios, respectively, confirming our theoretical predictions. The time derivative of $T(t)$ at $\Delta = 0$ is presented in Fig. 3c. Points A, B, and C correspond to the results in g-i, with point B being near the threshold-like transition point.

In order to further establish the analogy with conventional lasing mechanisms, inspired by the Schawlow-Townes formula[42] in laser physics, which describes the linewidth of laser emission below threshold, we investigated the relationship between the output and linewidth in our lasing-like dynamics below the threshold-like transition point (Supplementary Note 5). This analysis further validates the laser-like analogy of our system. We measured the amplitude

https://doi.org/10.1038/s41467-026-70123-w

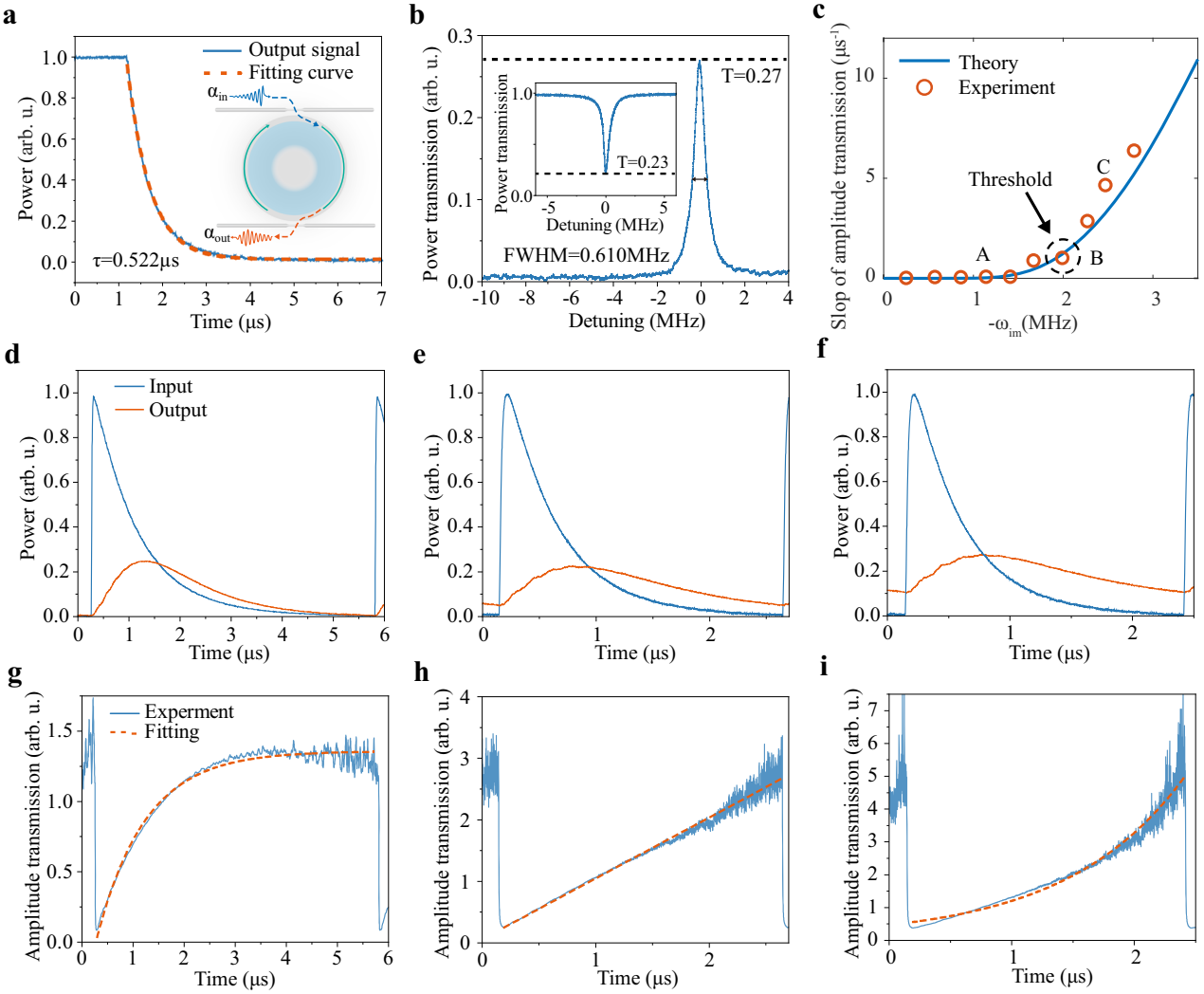

Fig. 3 | Experimental observation of lasing-like dynamics. a Cavity ring-down measurement, where the measured data (blue line) is fitted (red dashed line) to determine the lifetime of the cavity. Inset in **a**: Schematic diagram of the lasing-like dynamics experiment. **b** Measured power transmission spectrum at the drop port at real frequencies of the resonator. Inset in **b**: Measured power transmission spectrum at the through port. The intensity transmission peak at the drop port at zero detuning is 0.27, while the intensity transmission dip at the through port is 0.23. The estimated intrinsic loss and external coupling rates are $\kappa_i = 0.92MHz, \kappa_1 = 0.5MHz, \kappa_2 = 0.5MHz$, respectively. **c** Time derivative of $T(t)$ at $\Delta = 0$ and $t = -5.3/\omega_{im}$ plotted as a function of virtual gain. "Theory" refers to theoretical results calculated with the above parameters. **d**–**f** Experimentally obtained input and output pulse intensities at $\Delta = 0$ for various virtual gains corresponding to A, B, and C in **c**. **g**–**i** Time evolution of amplitude transmission coefficient corresponding to A, B, and C. Notably, the near-threshold situation is illustrated in **e** and **h**, and is marked in **c**.

transmittance in the quasi-steady state at different frequency detuning Δ (in the above discussion, we only consider $\Delta = 0$ and study the time evolution of transmittance) with different virtual gain $-\omega_{im}$ below the transition point. We focus on the peak value of the amplitude transmittance T_{peak} and the full width at half maximum (FWHM) $\Delta\omega_{3dB}$ of the power transmission spectrum. We selected a cavity mode with $\kappa_i = 0.85\text{MHz}, \kappa_1 = 0.48\text{MHz}, \kappa_2 = 0.48\text{MHz}$, and the experimental results are shown in Fig. 4. We show representative spectra for $-\omega_{im} = 0.187\text{MHz}$ and $-\omega_{im} = 1.02\text{MHz}$, respectively (Fig. 4a, b). The $\Delta\omega_{3dB}$ decreases from 3.13 MHz to 1.59 MHz as virtual gain increases, while T_{peak} increases from 0.547 to 1.334. Plotting T_{peak} and $\Delta\omega_{3dB}$ as functions of virtual gain is shown in Fig. 4c, we find that their product remains constant as $T_{peak}\Delta\omega_{3dB} = 4\sqrt{\kappa_1\kappa_2}$. This is analogous to the Schawlow-Townes formula, where linewidth is inversely proportional to output power. This confirms that below the transition point, our system exhibits laser-like spectral characteristics, further supporting its designation as a virtual analog of a laser operating below threshold.

Coexistence of CVA and lasing-like regime

In prior studies[17,18], virtual critical coupling has been achieved in an over-coupled microcavity excited by an exponentially growing signal, where virtual loss compensates for the discrepancy between intrinsic loss and the coupling rate. However, virtual critical coupling can also be realized using virtual loss when the resonant mode is initially under-coupled, and this phenomenon can be investigated at the through port in our system (Supplementary Note 4). Additionally, lasing-like behavior can also be observed at the through port. For simplicity, we employed another microcavity coupled to only one tapered fiber to analyze the output signal and transmission characteristics. The experimental setup is shown in Supplementary Fig. 3. The coupling state of the cavity-fiber system is tuned into the under-coupled regime by adjusting both the gap between the tapered fiber and the microcavity and the coupling position along the tapered region of the fiber. The inset of Fig. 5c displays the measured power transmission spectrum at real frequencies of the resonator. The FWHM is 0.759 MHz, corresponding to a total loss of

https://doi.org/10.1038/s41467-026-70123-w

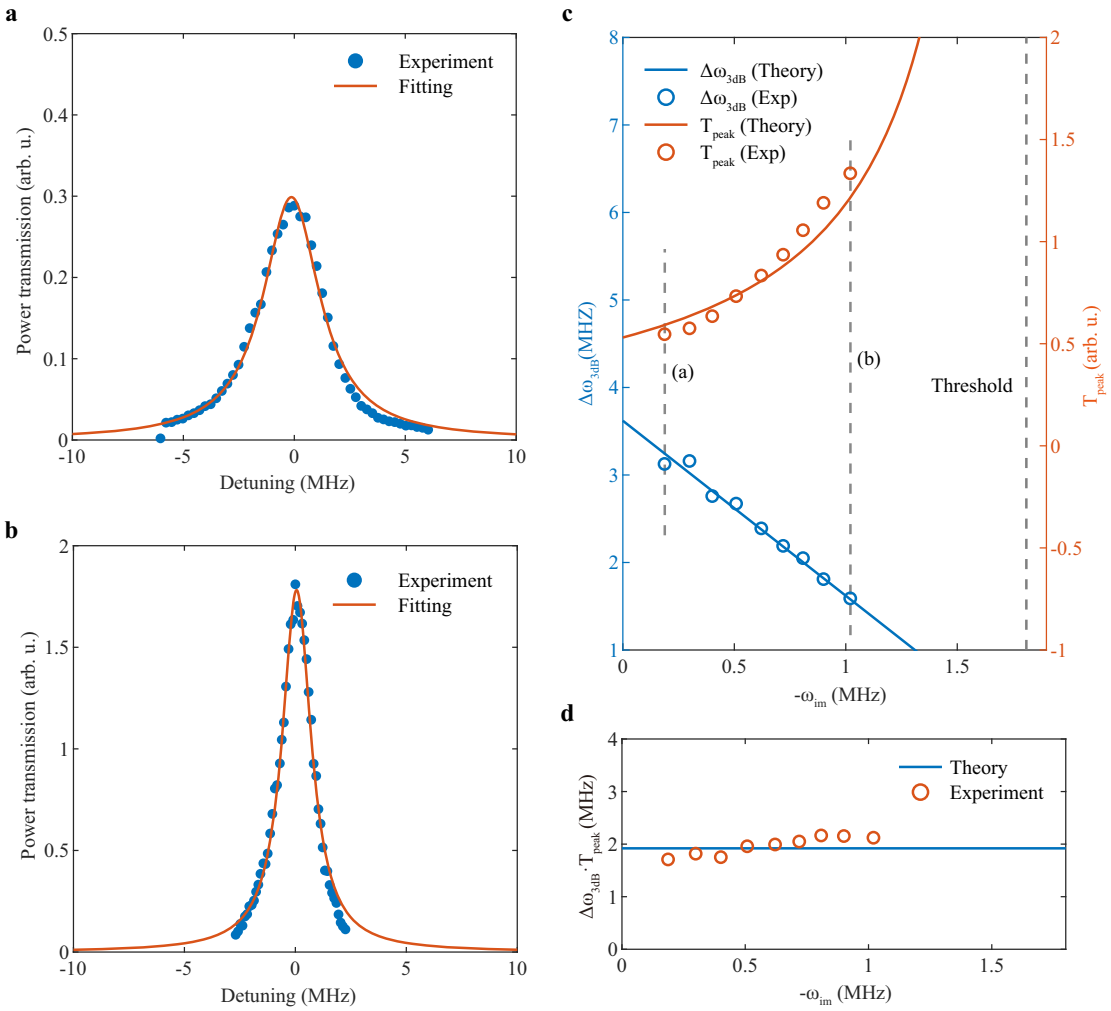

Fig. 4 | Schawlow–Townes-like relation between the peak transmittance and the spectral width. a Frequency response of the power transmission spectrum for $-\omega_{im} = 0.187MHz$. The FWHM is$\Delta\omega_{3dB} = 3.13MHz$, while the corresponding peak amplitude transmittance is $T_{peak} = 0.547$. **b** power transmission spectrum for $-\omega_{im} = 1.02MHz$. The FWHM is $\Delta\omega_{3dB} = 1.59MHz$, while the peak amplitude transmittance is $T_{peak} = 1.334$. All these results are obtained at $\kappa_i = 0.85MHz, \kappa_1 = 0.48MHz, \kappa_2 = 0.48MHz$. **c** $\Delta\omega_{3dB}$ and T_{peak} plotted as a function of virtual gain $-\omega_{im}$. As the virtual gain increases, T_{peak} increases, while $\Delta\omega_{3dB}$ gradually decreases. "Exp" means experimental results. **a**, **b** Refer to the condition shown in **a** and **b**. The threshold condition is also marked with dashed line. **d** The product of these two parameters, which remains constant.

$\kappa = 2.37$MHz. We can estimate the intrinsic loss and external coupling rate to be$\kappa_i = 1.79$MHz, $\kappa_{ex} = 0.58$MHz.

For an initially under-coupled cavity, the virtual gain compensates for the mismatch between intrinsic loss and coupling rate, and further compensates for the total loss if it is sufficiently large. Consequently, as the virtual gain increases, the system sequentially transitions through virtual under-coupling, virtual critical coupling, and virtual over-coupling, eventually reaching the lasing-like regime. We focused on the system's response and plotted the input and output pulses at various levels of virtual gain. The relative power transmission as a function of time for three selected complex excitation frequencies, corresponding to virtual under-coupling, virtual critical coupling, and virtual over-coupling, is shown in Fig. 5b. Additionally, the time evolution of amplitude transmission for the lasing-like behavior was measured and depicted in Fig. 5d. The intensity transmission in the quasi-steady state for different exponential decay rates is illustrated in Fig. 5a, where A ~ C corresponds to the three curves in b. Meanwhile, the time derivative of amplitude transmittance at $\Delta = 0$ was plotted as a function of virtual gain in Fig. 5c, where D and E correspond to the results in d. Both experimental results in the two scenarios are in excellent agreement with theoretical predictions.

Discussion

In summary, we have successfully demonstrated lasing-like dynamics in a passive system consisting of an ultra-high Q add-drop microcavity. The instantaneous amplitude transmittance, which is defined as the instantaneous ratio between output and input signals, displays three distinct amplification regimes during the pulse duration: saturable, linear, and exponential growth. The virtual gain introduced by the exponentially decaying excitation mimics the role of material gain in a conventional cavity, allowing access to complex frequency poles and compensating for the intrinsic loss in the open cavity, driving the system from a quasi-steady state to a regime of divergent response. This phenomenon is linear, hence does not showcase nonlinear gain saturation, yet it exhibits striking similarities to the dynamics of real lasers as they approach threshold, including a threshold-like transition and saturable/divergent transmittance amplification under tailored excitations. Our results extend the scope of coherent wave control into fully passive, dissipative systems, offering a versatile platform for studying and utilizing non-Hermitian wave phenomena. Furthermore, this framework enables CVA when analyzing the through port of an under-coupled cavity. As the virtual gain varies, both CVA and lasing-like response can be observed in the same system. These findings

https://doi.org/10.1038/s41467-026-70123-w

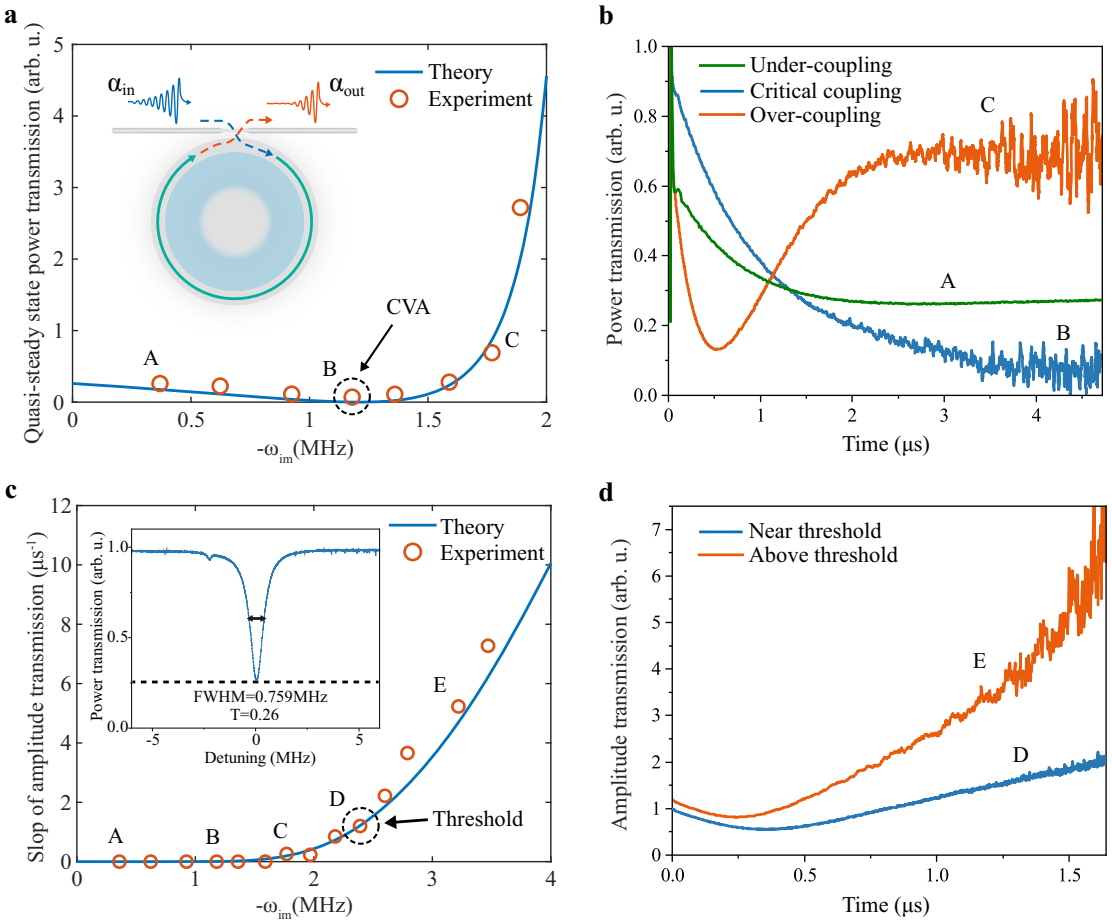

Fig. 5 | Transition from coherent virtual absorption to lasing-like response. **a** Transmission of the pulse in the quasi-steady state as a function of $-\omega_{im}$. Inset in **a**: Schematic diagram of the CVA experiment. **b** Power transmission for virtual under-coupling (green, $-\omega_{im} = 0.369MHz$), virtual critical coupling (blue, $-\omega_{im} = 1.18MHz$), and virtual over-coupling (red, $-\omega_{im} = 1.77MHz$), corresponding to A ~ C in **a**. **c** The time derivative of the time evolution of amplitude transmittance at $t = -5.3/\omega_{im}$ plotted as a function of $-\omega_{im}$. Inset in **c**: Measured power transmission spectrum at real frequencies of the resonator. The coupling state of the cavity-fiber system is tuned into the under-coupled regime via adjustment of the fiber position and gap. The estimated intrinsic loss and external coupling rate are $\kappa_i = 1.79MHz$, $\kappa_{ex} = 0.58MHz$ respectively. **d** Amplitude transmission for near transition point (blue, $-\omega_{im} = 2.39MHz$) and above transition (red, $-\omega_{im} = 2.61MHz$) situations, corresponding to D and E in **c**.

provide a simple and compact method for controlling light-matter interaction beyond the limits imposed by passivity, advancing the theoretical framework for the response of complex-frequency excitation in microcavities. By enabling on-demand switching among different absorbing and amplifying responses in a single passive microcavity, this platform provides a new route toward gain-free, reconfigurable signal control and offers a testbed for exploring non-Hermitian phenomena in integrated photonics, thus paving the way for various applications such as sensing, energy storage, and optical communication capabilities and positioning our work as a valuable contribution to these fields.

Methods

Measurement of lasing-like dynamics

Our microcavity was coupled to two tapered fibers, forming an add-drop microcavity system. A continuously tunable laser (NKT Photonics) was used as an optical source, whose wavelength can be precisely tuned around 1560 nm and is very stable. The laser was amplified by an EDFA. The intensity and polarization of this branch were controlled by a variable optical attenuator (VOA) and a polarization controller (PC), respectively. Then the continuous laser was modulated by an EOM (electro-optical modulator) to generate pulses with exponentially decaying profiles. We used another polarization controller to control the polarization of the pulse. The pulse was then divided by a 50:50 coupler. The signal at one channel was used to excite the WGM microcavity, while the other channel was used to monitor the profile of the input signal. Both the outcoupled signal and the monitor signal were detected by photodetectors (PD). The spectra were observed on an oscilloscope (OSC). We recorded the input and output pulse intensities for different imaginary frequencies and analyzed their time evolutions.

Ring-down measurement for evaluating Q factor

A ring-down measurement was performed to determine the Q factor of the resonator. We launched a square wave pulse with a sharp falling edge into the cavity, allowing us to extract the cavity lifetime from the decaying optical fields at the falling edge of the pulse. We monitored the transmission at zero detuning using a photodetector. The lifetime τ of the resonator was evaluated by fitting an exponential decay function to the output signal. The loaded Q factor and the total loss can be calculated using $Q = \omega\tau/2$. Here, the bandwidth of our EOM was 40 GHz, which corresponds to 25 ps. It is much smaller than the cavity lifetime. As a result, the EOM does not appreciably affect the measurement.

Sample fabrication

The CaF_2 microcavity used in our experiment has a diameter of 1 millimeter and a thickness of 0.5 millimeter. It was fabricated through precise polishing and has an ultra-high Q-factor of $10^8 \sim 10^9$. Firstly, a centimeter-sized CaF_2 wafer was affixed to a stainless-steel rod using UV-curing glue. Then, the rod was precisely mounted onto a ball bearing lathe and rotated by a motor with adjustable speed. Aluminum oxide sandpapers with varying grits of 600, 1200, 1500, 2000, and 5000 were successively employed to shape the resonator until we achieved the desired size without noticeable scratches on the sample surface. Afterwards, the rim surface of the sample was manually polished using polishing cloths assisted by diamond suspensions with different particle sizes. In our fabrication procedure, 1 μm, 0.25 μm, 0.1 μm, and 0.05 μm suspensions were used subsequently to achieve an extremely smooth rim. Each step lasted for about 20 min. The sample should be carefully cleaned with anhydrous ethanol and deionized water after each step. Finally, a thorough cleaning procedure with a 3-min water flow and acetone soaking was applied. This microcavity was coupled to two tapered fibers, which were fabricated from standard single-mode fibers in the telecom band (G.652.D), forming an add-drop microcavity system. The entire device was placed inside a vacuum-sealed metal box to ensure environmental stability.

Reporting summary

Further information on research design is available in the Nature Portfolio Reporting Summary linked to this article.

Data availability

The data generated in this study are available in the main article, Supplementary Information, and Source Data file. The data are also available from the authors. Source data are provided with this paper.

References

1. Haus, H. *Waves and Fields in Optoelectronics* (Prentice-Hall, 1984).
2. Grigoriev, V. et al. Singular analysis of Fano resonances in plasmonic nanostructures. *Phys. Rev. A* **88**, 063805 (2013).
3. Fan, S., Suh, W. & Joannopoulos, J. D. Temporal coupled-mode theory for the Fano resonance in optical resonators. *J. Opt. Soc. Am. B* **20**, 569–572 (2003).
4. Chong, Y. D., Ge, L., Cao, H. & Stone, A. D. Coherent perfect absorbers: time-reversed lasers. *Phys. Rev. Lett.* **105**, 053901 (2010).
5. Baranov, D. G., Krasnok, A. & Alu, A. Coherent virtual absorption based on complex zero excitation for ideal light capturing. *Optica* **4**, 1457–1461 (2017).
6. Ra'di, Y., Krasnok, A. & Alù, A. Virtual critical coupling. *ACS Photonics* **7**, 1468–1475 (2020).
7. Kim, S., Krasnok, A. & Alù, A. Complex-frequency excitations in photonics and wave physics. *Science* **387**, eado4128 (2025).
8. Longhi, S. Coherent virtual absorption for discretized light. *Opt. Lett.* **43**, 2122–2125 (2018).
9. Novitsky, D. V. Tunable virtual gain in resonantly absorbing media. *Phys. Rev. A* **107**, 013516 (2023).
10. Gu, Z. et al. Transient non-Hermitian skin effect. *Nat. Commun.* **13**, 7668 (2022).
11. Trainiti, G., Ra'di, Y., Ruzzene, M. & Alù, A. Coherent virtual absorption of elastodynamic waves. *Sci. Adv.* **5**, eaaw3255 (2019).
12. Li, H., Mekawy, A., Krasnok, A. & Alù, A. Virtual parity-time symmetry. *Phys. Rev. Lett.* **124**, 193901 (2020).
13. Yang, X. et al. Observation of transient parity-time symmetry in electronic systems. *Phys. Rev. Lett.* **128**, 065701 (2022).
14. Marini, A. V., Ramaccia, D., Toscano, A. & Bilotti, F. Perfect matching of reactive loads through complex frequencies: from circuital analysis to experiments. *IEEE Trans. Antenn. Propag.* **70**, 9641–9651 (2022).
15. Delage, T., Pascal, O., Sokoloff, J. & Mazières, V. Experimental demonstration of virtual critical coupling to a single-mode microwave cavity. *J. Appl. Phys.* **132**, 153105 (2022).
16. Delage, T. et al. Plasma ignition via high-power virtual perfect absorption. *ACS Photonics* **10**, 3781–3788 (2023).
17. Krasnok, A., Baranov, D. G., Generalov, A., Li, S. & Alù, A. Coherently Enhanced Wireless Power Transfer. *Phys. Rev. Lett.* **120**, 143901 (2018).
18. Marini, A., Ramaccia, D., Toscano, A. & Bilotti, F. Metasurface bounded open cavities supporting virtual absorption: free space energy accumulation in lossless systems. *Opt. Lett.* **45**, 3147–3150 (2020).
19. Hinney, J. et al. Efficient excitation and control of integrated photonic circuits with virtual critical coupling. *Nat. Commun.* **15**, 2741 (2024).
20. Zhong, Q., Simonson, L., Kottos, T. & El-Ganainy, R. Coherent virtual absorption of light in microring resonators. *Phys. Rev. Res.* **2**, 013362 (2020).
21. Araujo-Martinez, A. C., Krasnok, A., Kutsaev, S. V., Seltzman, A. H., Smirnov, A. Y. Virtual critical coupling in high-power resonant systems. *IEEE Transactions on Plasma Science* (2025).
22. Ferise, C., del Hougne, P. & Davy, M. Optimal matrix-based spatio-temporal wave control for virtual perfect absorption, energy deposition, and scattering-invariant modes in disordered systems. *Phys. Rev. Appl.* **20**, 054023 (2023).
23. Chen, L., Kottos, T. & Anlage, S. M. Perfect absorption in complex scattering systems with or without hidden symmetries. *Nat. Commun.* **11**, 5826 (2020).
24. Novitsky, D. V. & Shalin, A. S. Virtual perfect absorption in resonant media and their PT-symmetric generalizations. *Phys. Rev. A* **108**, 053513 (2023).
25. Farhi, A. et al. Excitation of absorbing exceptional points in the time domain. *Phys. Rev. A* **106**, L031503 (2022).
26. Lepeshov, S. & Krasnok, A. Virtual optical pulling force. *Optica* **7**, 1024–1030 (2020).
27. Kim, S., Lepeshov, S., Krasnok, A. & Alù, A. Beyond bounds on light scattering with complex frequency excitations. *Phys. Rev. Lett.* **129**, 203601 (2022).
28. Kim, S., Peng, Y.-G., Yves, S. & Alù, A. Loss compensation and superresolution in metamaterials with excitations at complex frequencies. *Phys. Rev. X* **13**, 041024 (2023).
29. Guan, F. et al. Overcoming losses in superlenses with synthetic waves of complex frequency. *Science* **381**, 766–771 (2023).
30. Guan, F. et al. Compensating losses in polariton propagation with synthesized complex frequency excitation. *Nat. Mater.* **23**, 506–511 (2024).
31. Archambault, A., Besbes, M. & Greffet, J. J. Superlens in the time domain. *Phys. Rev. Lett.* **109**, 097405 (2012).
32. Hou, J. et al. Self-induced transparency in a perfectly absorbing chiral second-harmonic generator. *PhotoniX* **3**, 22 (2022).
33. Xue, B. et al. Dual-color coherent perfect absorber. *Phys. Rev. Lett.* **134**, 013802 (2025).
34. Wan, W. et al. Time-reversed lasing and interferometric control of absorption. *Science* **331**, 889–892 (2011).
35. Tetikol, H. S. & Aksun, M. I. Enhancement of resolution and propagation length by sources with temporal decay in plasmonic devices. *Plasmonics* **15**, 2137–2146 (2020).
36. Kirby, E., Hamm, J., Pickering, T., Tsakmakidis, K. & Hess, O. Evanescent gain for slow and stopped light in negative refractive index heterostructures. *Phys. Rev. B* **84**, 041103 (2011). R.
37. Ciattoni, A., Marini, A., Rizza, C., Scalora, M. & Biancalana, F. Polariton excitation in epsilon-near-zero slabs: transient trapping of slow light. *Phys. Rev. A* **87**, 053853 (2013).
38. Tsakmakidis, K. L. et al. Completely stopped and dispersionless light in plasmonic waveguides. *Phys. Rev. Lett.* **112**, 167401 (2014).

39. Tsakmakidis, K. L., Baskourelos, K. G., Wartak, M. S. *Metamaterials and Nanophotonics* (World Scientific, 2022).
40. Zeng, K. et al. Synthesized complex-frequency excitation for ultra-sensitive molecular sensing. *eLight* **4**, 1 (2024).
41. Zheng, Y. et al. Optically induced transparency in a micro-cavity. *Light Sci. Appl.* **5**, e16072 (2016).
42. Schawlow, A. L. & Townes, C. H. Infrared and optical maser. *Phys. Rev.* **112**, 1940 (1958).

Acknowledgements

W.W. and his group were supported by the Shanghai Technology Innovation Project (No. 24590711300; No. 25JD1405800); the National Science Foundation of China (Grant No. 12274295, No. 92050113); Shanghai Institute for Mathematics and Interdisciplinary Sciences (SIMIS-ID-2025-QT); the National Key Research and Development Program (Grant No. 2023YFB3906400, No. 2023YFA1407200). A.A. was supported by the Simons Foundation.

Author contributions

W.W. initiated the idea and designed the study; A.A. provided theoretical guidance. W.W., A.A., X.C. supervised the work; B.X. performed experimental work; R.Z., Y.Z., and Y.S. helped analyze the data and discussion; W.W., B.X., and A.A. wrote the paper; All authors reviewed the manuscript.

Competing interests

The authors declare no competing interests.

Additional information

Supplementary information The online version contains supplementary material available at https://doi.org/10.1038/s41467-026-70123-w.

Correspondence and requests for materials should be addressed to Andrea Alù or Wenjie Wan.

Peer review information *Nature Communications* thanks Mostafa Honari-Latifpour and the other, anonymous, reviewer(s) for their contribution to the peer review of this work. A peer review file is available.